Gate-tunable Casimir equilibria with transparent conductive oxides

Lixin Ge,[1,*] Xi Shi,[2] Liang Liu,[3] and Ke Gong[1]
[1]*School of Physics and Electronic Engineering, Xinyang Normal University, Xinyang 464000, China*
[2]*Department of Physics, Shanghai Normal University, Shanghai, 200234, China*
[3]*College of Math and Physics, Mianyang Normal University, Mianyang, Sichuan 621000, China*

(Received 30 March 2020; revised 29 July 2020; accepted 30 July 2020; published 12 August 2020)

The active control of small particles due to the Casimir force is of great interest for noncontact and low-friction micro- and nanoelectromechanical systems (MEMS and NEMS). In this work, we study theoretically the Casimir force between a nanoplate and a metal-oxide-semiconductor (MOS) substrate immersed in a liquid environment. The MOS structure consists of layers indium-tin-oxide (ITO)/Teflon/Au, where a gate electrode is connected between the ITO film and the gold substrate. Our results suggest that the Casimir equilibria are determined, not only by the layer thicknesses in MOS structures but also by the carrier densities of ITO (gate-controllable). Under proper conditions, a gold nanoplate can be stably trapped due to the Casimir forces. Moreover, we show that the trapping state can be released by decreasing the carrier density in the active layer of ITO, e.g., from 10^{21} to 10^{19} cm^{-3}. The switching between stable trapping and the release state of a suspended Teflon nanoplate is also demonstrated. Our findings can be useful in designing ultrafast switchable devices for applications in MEMS/NEMS.

DOI: 10.1103/PhysRevB.102.075428

I. INTRODUCTION

The Casimir force is a macroscopic quantum effect due to the fluctuations of the electromagnetic field [1]. It has been confirmed experimentally that the Casimir forces between two metallic objects are attractive (see the review [2] and recent progress [3,4]). In the wrong hands, the attractive Casimir forces can be adverse for micro- and nanoelectromechanical systems (MEMS and NEMS) [5], due to the caused stiction at nanoscale separations [6,7]. With that in mind, repulsive Casimir forces are proposed and investigated for noncontact and low-friction MEMS and NEMS based on various materials [8–15]. It is known that the Casimir forces between two liquid-separated objects (labelled 1 and 2) can be repulsive when the permittivity satisfies $\varepsilon_1(i\xi) > \varepsilon_{\rm liq}(i\xi) > \varepsilon_2(i\xi)$ for a vast range of frequency [16,17], where $\varepsilon_{\rm liq}(i\xi)$ is the permittivity of the intervening liquid evaluated with imaginary frequency $\omega = i\xi$. The balances between repulsive and attractive Casimir forces give rise to Casimir equilibria. In certain configurations, stable Casimir equilibria (or called quantum trapping) can be realized using the enclosed geometries [18,19] and dispersive materials [20,21]. Recently, stable Casimir equilibria were reported experimentally by Zhao *et al.*, based on a Teflon-coated gold substrate [22]. Although considerable progress has been made, not much attention has been paid to the question of how Casimir equilibria can actively be controlled. The trapping properties due to Casimir forces are difficult to be changed once the devices are fabricated. For that reason, tunable Casimir equilibria or even the switching from quantum trapping to its release by external stimuli (e.g., heating, electrical gating, or optical waves) are of great interest in MEMS and NEMS.

To tune the Casimir forces, one straight scheme indicated by the Lifshitz theory [23] is to modulate the dielectric functions of materials actively. Indeed, there are several pioneer works carried out with this mind. In 2007, Chen *et al.* showed that Casimir forces could be modified under an applied laser [24]. The modification is related to the change of charge-carrier density(i.e., the dielectric functions) in doped semiconductors under an optical lasing. In 2011, Chang *et al.* reported that Casimir forces can be modulated after the UV treatment on indium-tin-oxide (ITO) films [25], although the underlying mechanism for the modulation is still a controversy nowadays [26,27]. The modulations of Casimir forces between graphene sheets were also reported due to the change of conductivities under external stimuli [28–31]. Another outstanding scheme to control the Casimir force is based on phase change materials (PCMs) [32–34]. The optical properties of PCMs change dramatically during the phase transition under external control (e.g., heating and optical pumps). It was reported that the Casimir forces could be modified considerably as the phase transitions occur in PCM of $Ag_5In_5Sb_{60}Te_{30}$ (AIST) [32,33]. In 2018, M. Boström *et al.* showed that the Casimir force can be switched between attraction and repulsion with PCM of tin [34]. In addition, the PCM of VO_2 was also used to modulate the magnitude of Casimir forces [35–38]. Recently, we proposed the idea of tunable Casimir forces in a liquid environment, using PCM of VO_2 [39]. Not only the magnitude of the Casimir force can be modified, but also the sign (e.g., from attraction to repulsion) can be switched. As a result, the switching between quantum trapping of a nanoplate and its release is possible due to the phase transition of VO_2 [39]. However, the transition temperature T_c around 340 K could be

*lixinge@hotmail.com

a constraint for some liquids whose boiling points are lower than T_c.

The metal-oxide-semiconductor (MOS) devices are basic building blocks in modern electronics. The MOS devices can also provide an excellent platform for kinds of electro-optic modulations [40–43], resulting from the dramatic change of the carrier density in semiconductors with an ultrahigh speed. In present work, we aim to theoretically design gate-tunable Casimir equilibria by a ITO-based MOS systems. There is a gate electrode connected between the ITO layer and the gold substrate. As the voltage is applied, an active layer forms between the ITO/Teflon interface. The density of electron at the active layer is modulated by the gate electrode, resulting in a dynamic control of Casimir forces. Remarkably, we find that a switch from quantum trapping of the gold nanoplate("on" state) to its release ("off" state) can be realized as the carrier density decreases in the active layer. In addition to gold nanoplates, the gate-tunable Casimir equilibria of Teflon nanoplates are also demonstrated. Instead, we find that a switch from quantum trapping to its release can be induced as the carrier density increases, e.g., from 10^{19} to 10^{21} cm^{-3}, which is accessible in nowadays experiments.

II. THEORETICAL MODELS

The system under study is schematically shown in Fig. 1. We consider a gold nanoplate with thickness L_0 is suspended in a liquid environment of bromobenzene. The bromobenzene can be considered as a high-refractive-index liquid and its melting point is around 240 K. The substrate is a multilayer stack, and it consists of a Teflon film deposited on the MOS structure of ITO/Teflon/gold. There is an active layer located next to the interface between the ITO and the Teflon. The

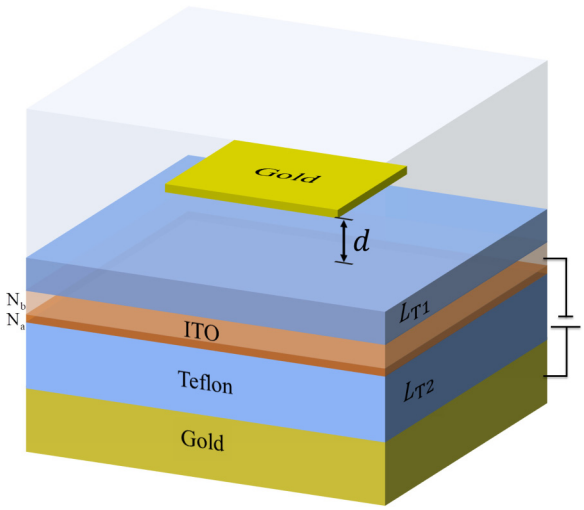

FIG. 1. Schematic view of a gold nanoplate suspended in a liquid environment. The separation between the gold nanoplate and the substrate is d. The substrate consists of a Teflon film deposited on the MOS structure of ITO/Teflon/gold. An electrical gating is connected between the layers of ITO and gold. The carrier densities for the active and nonactive (background) layers of ITO are denoted as N_a and N_b. The magnitude of N_a is controlled by the applied gating, leading to the modulation of Casimir forces.

layer thicknesses (from top to down) for the top-layer Teflon, background ITO, active ITO, and middle Teflon are denoted as L_{T1}, $L_I - L_a$, L_a, and L_{T2}, respectively. Here, L_a is set as a typical value of 1 nm [40,43]. The carrier density in the active layer (denoted N_a) is considered homogeneous, and its accumulation (or depletion) is controlled by external voltage gating. For simplicity, the proximity force approximation (PFA) is applied for the calculations because of the in-plane dimension is much larger than the separation d. The Casimir force is calculated by $F_c = -\partial E_c(d)/\partial d$, where $E_c(d)$ is the Casimir energy between the gold nanoplate and the substrate, having the form [15,22]

$$E_c(d) = A\hbar \int_0^\infty \frac{d\xi}{2\pi} \int \frac{d^2\mathbf{k}_\parallel}{(2\pi)^2} \log\det[1 - \mathbf{R_1} \cdot \mathbf{R_2} e^{-2K_l d}], \tag{1}$$

where $\hbar$ is the reduced Planck constant, A represents the in-plane area, $\mathbf{k}_\parallel$ is the parallel wave vector, $K_l = \sqrt{k_\parallel^2 + \varepsilon_{\rm liq}(i\xi)\xi^2/c^2}$ is the vertical wave vector in the liquid, c is the speed of light in vacuum, $\mathbf{R}_{1,2}$ is the 2×2 reflection matrix, given by

$$\mathbf{R_j} = \begin{pmatrix} r_j^s & 0 \\ 0 & r_j^p \end{pmatrix}, \tag{2}$$

where r_j with $j = 1$ and $j = 2$ are the reflection coefficients for the upper and lower layered structures, and the superscripts s and p correspond to the polarization of transverse electric (**TE**) and transverse magnetic (**TM**) modes, respectively. For a nanoplate suspended in a liquid, the reflection coefficients can be given analytically as follows [12]

$$r^\alpha = \frac{r_{0j}^\alpha + r_{j0}^\alpha e^{-2K_j L_0}}{1 + r_{0j}^\alpha r_{j0}^\alpha e^{-2K_j L_0}}, \tag{3}$$

where $\alpha = s$ and p, $K_j = \sqrt{k_\parallel^2 + \varepsilon_j(i\xi)\xi^2/c^2}$ with $\varepsilon_j(i\xi)$ being the permittivity of the nanoplate. The subscripts of r_{mn}^α represent the light is incident from the medium m to n (0 means the liquid). Alternatively, the reflection coefficients for layered structures can be calculated by a transfer matrix method. The general form is given as $r = M_{21}/M_{11}$, where M_{21} and M_{11} are the elements of the M matrix [44]. The M matrix is the multiplications of transmission matrices across different interfaces and propagation matrices in different layers. If we consider an arbitrary N-layer system, the M matrix is given as:

$$M = D_{0,1}P(L_1)D_{1,2}P(L_2)...D_{N-1,N}P(L_N)D_{N,N+1}, \tag{4}$$

where $L_j (j = 1, 2, 3...)$ is the thickness of the jth layer, the transmission matrix $D_{j,j+1}$ is given as:

$$D_{j,j+1} = \frac{1}{2}\begin{bmatrix} 1+\eta & 1-\eta \\ 1-\eta & 1+\eta \end{bmatrix}, \tag{5}$$

where $\eta = \varepsilon_j(i\xi)K_{j+1}/(\varepsilon_{j+1}(i\xi)K_j)$ for the p polarization and $\eta = K_{j+1}/K_j$ for the s polarization. For the s and p polarizations, the propagation matric in the jth layer is all written as:

$$P(L_j) = \begin{bmatrix} e^{K_j L_j} & 0 \\ 0 & e^{-K_j L_j} \end{bmatrix}. \tag{6}$$

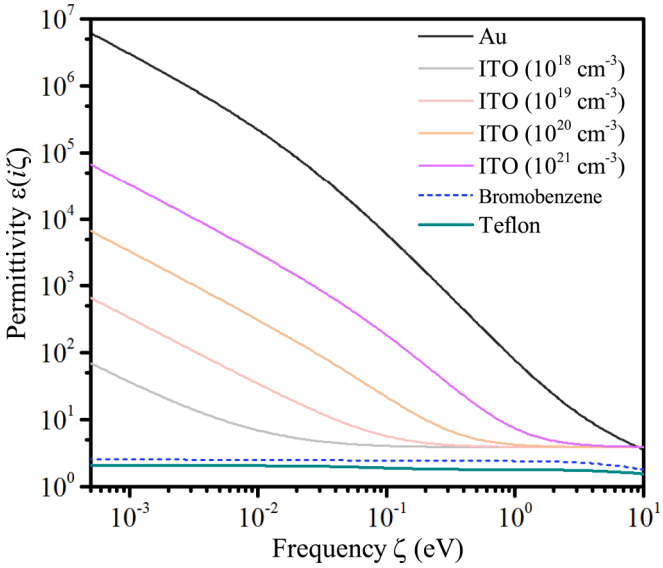

FIG. 2. The permittivity of gold, bromobenzene, doped ITO, and Teflon as a function of imaginary frequency.

For example, we have a layer number $N = 4$ for the multilayered substrate in Fig. 1. The M matrix is written as $M = D_{0,1}P(L_1)D_{1,2}P(L_2)D_{2,3}P(L_3)D_{3,4}P(L_4)D_{4,5}$, where the subscripts 0, 1, 2, 3, 4, and 5 represent the media of liquid, Teflon, background ITO, active ITO, Teflon and gold (from top to down), and the thicknesses $L_1 = L_{T1}, L_2 = L_I - L_a, L_3 = L_a, L_4 = L_{T2}$.

The dielectric functions of materials are significant for designing the Casimir forces. Here, the generalized Drude-Lorentz model is applied for gold, where four pairs of Lorentz poles are taken into account [45]. The permittivity for the bromobenzene and Teflon are fitted by the oscillator model [17]:

$$\varepsilon(i\xi) = 1 + \sum_j \frac{C_j}{1 + (\xi/\omega_j)^2}, \tag{7}$$

where C_j corresponds to the oscillator strength for the jth resonance frequency ω_j. There are seven (eight) resonant terms for the permittivity of bromobenzene (Teflon), and the values of the parameters (C_j and ω_j) can be found in Refs. [17,39]. On the other hand, the permittivity for the doped ITO is given by the Drude model [40]:

$$\varepsilon(i\xi) = \varepsilon_\infty + \frac{\omega_p^2}{\xi^2 + \xi\gamma_p}, \tag{8}$$

where $\varepsilon_\infty = 3.9$ is the high-frequency permittivity, $\gamma_p = 1.8 \times 10^{14}$ rad/s is the electron relaxation frequency, $\omega_p = \sqrt{Ne^2/\varepsilon_o m^*}$ is the plasma frequency and N represents the charge carrier density, e and ε_o denotes electron charge and the permittivity of vacuum, and $m^* = 0.35\, m_e$ is the effective mass of charge carriers with m_e being the electron mass.

III. RESULTS AND DISCUSSIONS

Figure 2 shows the dielectric functions of employed materials in this work. Obviously, the permittivity $\varepsilon(i\xi)$ of gold has a highest value for a broad range of frequencies, which can be considered as a high-quality mirror. The Teflon is a low-refractive-index material because its permittivity is smallest. As a result, the Casimir force is long-range repulsive for the layer structure of gold/bromobenzene/Teflon. Instead, the Casimir force for the structure of gold/bromobenzene/ITO is long-range attractive according to the permittivity of the materials. For a doped ITO, the dielectric functions change dramatically under different carrier densities. The permittivity, especially in the low frequency, increases significantly as the carrier density N increases from 10^{18} to 10^{21}cm^{-3}, providing a possibility to actively tune Casimir forces.

A. Gate-tunable Casimir pressures for gold nanoplates

Now we consider the Casimir pressure (denoted as $P_c = F_c/A$) between the gold nanoplate and the multilayered substrate in Fig. 1. To begin, we assume the applied voltage is zero and the carrier density is homogeneous in the ITO film, i.e., $N_a = N_b = N$. The layer thicknesses play an important role in the Casimir pressure as illustrated in Fig. 3. The upper panel shows the configuration of changing the thickness of ITO, while the top-layer Teflon with $L_{T1} = 10$ nm is fixed. For the density $N = 10^{19}$ cm^{-3} in Fig. 3(a), the Casimir pressure can be long-range repulsive for a vast choice of L_I, e.g., between 0 and 18 nm. As N increases to 10^{20} cm^{-3} [Fig. 3(b)], however, the long-range repulsion is achieved only when L_I is at the regime between 0 and 11 nm. Interestingly, the Casimir equilibria denoted by the black curves can be found under specific thicknesses. As the density N increases to 10^{21} cm^{-3} [Fig. 3(c)], the long-range repulsion is possible only when the thickness of ITO film is from 0 to about 2 nm. The upper panel suggests that the Casimir pressure tends to be attraction as the thickness of ITO increases. In addition, the increase of carrier density makes the ITO behaviors more like metal, which can enhance the attraction eventually.

On the other hand, the Casimir interaction between the gold nanoplate and the top-layer Teflon is repulsive. Quantitatively, the influences of the thickness of the top-layer Teflon on Casimir pressure are shown in the bottom panel of Fig. 3, where $L_I = 10$ nm is fixed. As the density $N = 10^{19}$ cm^{-3}, the Casimir pressure is long-range repulsive when the thickness L_{T1} is larger than about 6 nm. As N increases to 10^{20} cm^{-3}, the long-range repulsion is achieved only when the thickness L_{T1} is larger than 9 nm. For a high density 10^{21} cm^{-3}, the critical thickness for the long-range repulsion is even larger. The results indicate that the Casimir pressure tends to be repulsive as the thick L_{T1} increases. Again, the increasing of N makes the whole Casimir force be more attractive. To switch the nanoplate between quantum trapping and the release state, the delicate choices of the thickness of ITO and Teflon film are required.

Without loss of generality, we adopt the parameters $L_{T1} = L_I = 10$ nm for the concept of Casimir switching between quantum trapping and its release. Compared with the layer thicknesses, tuning the carrier density is more accessible in a real experiment. The Casimir pressures as a function of carrier density ($N_a = N_b = N$) are shown in Fig. 4(a), where the separations $d = 50$, 100, and 200 nm are calculated for demonstration. The results indicate that the Casimir pressures

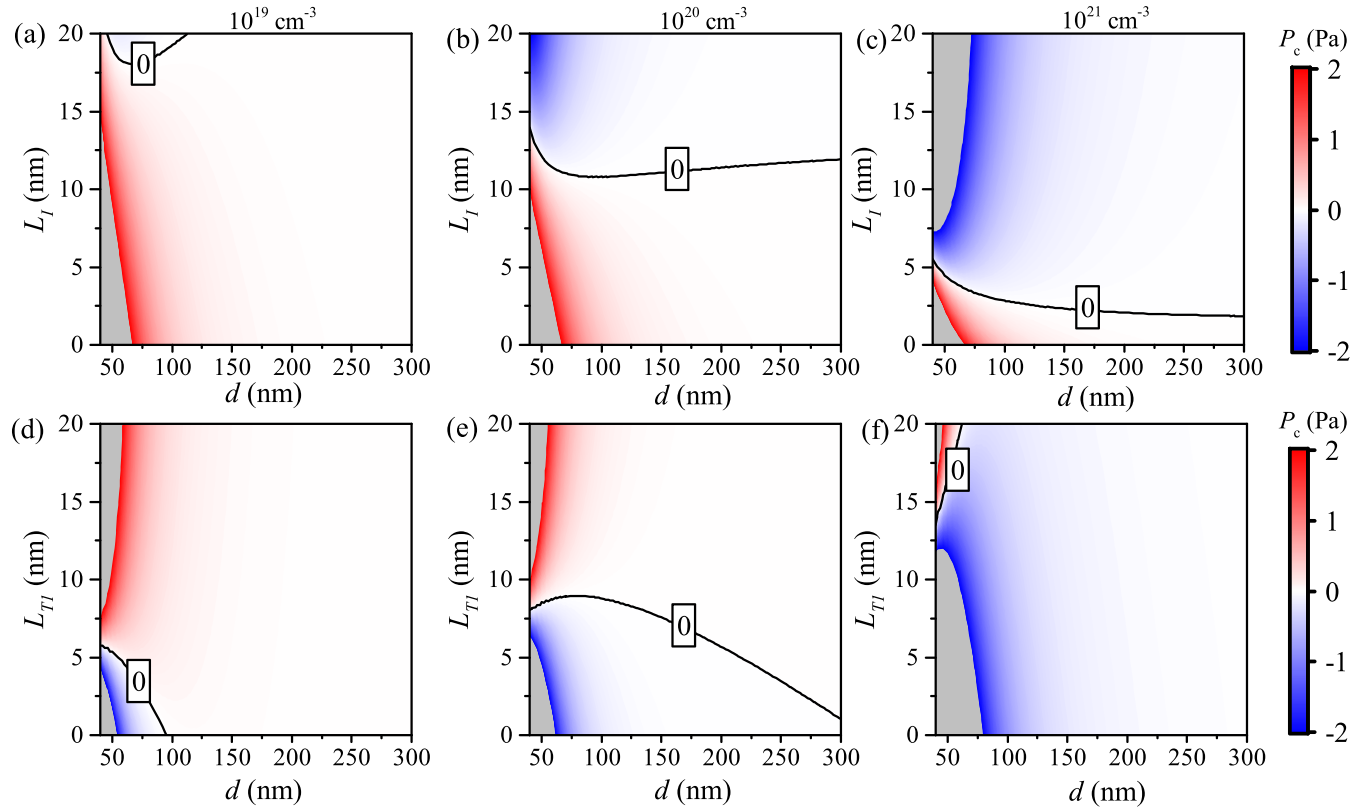

FIG. 3. Casimir pressure via layered thicknesses of ITO and top-layer Teflon without any applied voltage ($N = N_a = N_b$). In (a) and (d) $N = 10^{19}$ cm^{-3}; (b) and (e) $N = 10^{20}$ cm^{-3}; (c) and (f) $N = 10^{21}$ cm^{-3}. The black curves represent the Casimir equilibria (zero pressure). The positive (or negative) sign of the pressure corresponds to the repulsive(or attractive) force, and the gray zones represent the Casimir pressure with a magnitude larger than 2 Pa. The thickness $L_{T2} = 1000$ nm is fixed.

tend to be repulsive when the carrier density N is low. The variations of Casimir pressure are small as the density N increases from 10^{17} cm^{-3} to 10^{19} cm^{-3}. Notably, the Casimir equilibria can be found as N increases further to critical values. The critical density (about 1.2×10^{20} cm^{-3}) is almost the same for the separations 100 nm to 200 nm, indicating the large modulation of equilibrium distance d_c due to even very small variation of density. Overall, the Casimir pressure becomes attractive as the carrier density becomes a high value (e.g., $N = 10^{21}$ cm^{-3}).

The carrier densities for the background and active ITO could be different (i.e., $N_a \neq N_b$) as an gate voltage is applied. The Casimir pressure via different N_a are shown in Figs. 4(b) and 4(c). For background density $N_b = 10^{19}$ cm^{-3},

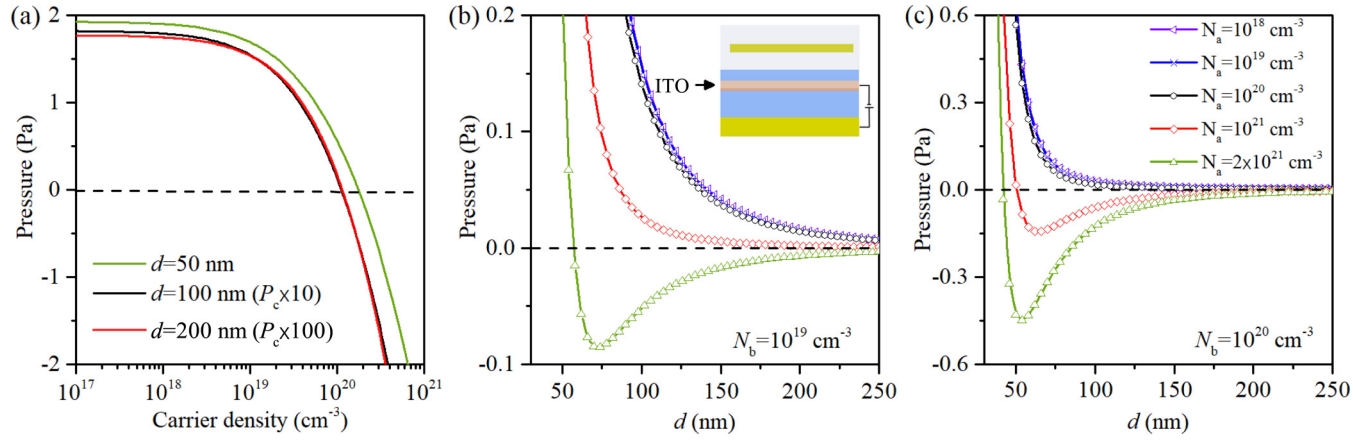

FIG. 4. Tunable Casimir equilibria for a suspended gold nanoplate. (a) Casimir pressure via the carrier density of ITO without any applied voltage ($N = N_a = N_b$). The magnitudes for separations $d = 100$ and 200 nm have been amplified 10 and 100 times. The Casimir pressure under different values of N_a, where the background density N_b is (b) 10^{19} cm^{-3} and (c) 10^{20} cm^{-3}, respectively. The positive (or negative) sign of the pressure corresponds to the repulsion (or attraction). The thicknesses parameters are set as $L_{T1} = 10$ nm, $L_I = 10$ nm, and $L_{T2} = 1000$ nm.

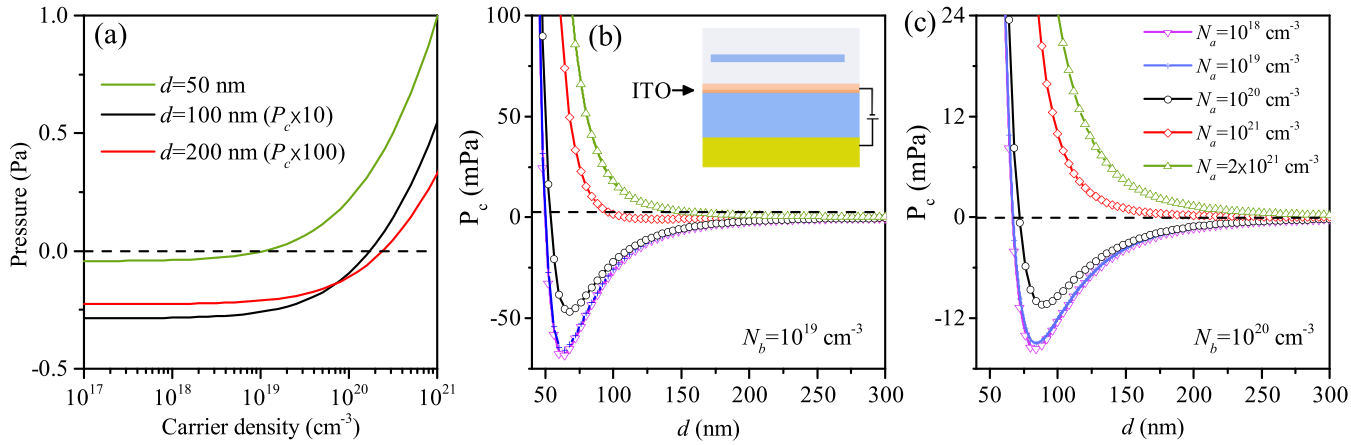

FIG. 5. Tunable Casimir equilibria for a suspended Teflon nanoplate with thickness of 100 nm. (a) Casimir pressure as a function of carrier density without electrical gating. (b) and (c) show Casimir pressures versus different active carrier densities, where the background density N_b are 10^{19} cm^{-3} and 10^{20} cm^{-3}, respectively. Note that the pressure P_{GB}, i.e., the sum of the gravity and buoyancy for the Teflon nanoplate, is only 0.6 (mPa). The thicknesses parameters are set as $L_{T1} = 0$ nm, $L_I = 5$ nm, and $L_{T2} = 1000$ nm.

the Casimir pressure is long-range repulsive without gating (i.e., $N_a = N_b$). As the density N_a is depleted to 10^{18} cm^{-3}, the pressure is almost unchanged in comparison with that of no-gating configuration. As the density N_a increases to 10^{20} cm^{-3}, the Casimir pressure decreases slightly comparing with the no-gating configuration. While the Casimir pressure drops greatly as $N_a = 10^{21}$ cm^{-3}. Interestingly, the Casimir equilibrium and stable quantum trapping can be obtained as N_a increases to 2×10^{21} cm^{-3}. Thus, a switching from long-range repulsion to quantum trapping can be realized by increasing the carrier density in the active layer of ITO, e.g., from 10^{19} to 2×10^{21} cm^{-3}, and vice versa. Another example with background density $N_b = 10^{20}$ cm^{-3} is shown in Fig. 4(c). The results indicate that the Casimir pressure is long-range repulsive without gating. As the density N_a depletes to 10^{18} and 10^{19} cm^{-3}, the curves of Casimir pressures for these two cases also overlaps. However, the Casimir equilibria and stable quantum trapping can be obtained as N_a increases to a high level, i.e., 10^{21} and 2×10^{21} cm^{-3}.

B. Gate-tunable switching for Teflon nanoplates

The manipulations of low-refractive-index nanoplates due to Casimir forces are also interesting in MEMS and NEMS. The schematic of our design is shown in the inset of Fig. 5. Inspiring by the previous work [39], the top layer of the multilayered substrate is set as an ITO film (i.e., $L_{T1} = 0$). Figure 5(a) shows the Casimir pressure as a function of carrier densities without any voltage bias. The results indicate that the Casimir pressure is attractive(or repulsive) when the carrier density of ITO is low (or high). Interestingly, the Casimir pressure is almost unchanged as the carrier density N increases from 10^{17} cm^{-3} to 10^{18} cm^{-3}. However, the pressure decreases and Casimir equilibria can be obtained as N increases further. The critical density for separation of 50 nm is about 10^{19} cm^{-3}, while the required densities become larger if the separation increases to 100 nm and 200 nm.

Figure 5(b) shows the Casimir pressures under different N_a, where the background density $N_b = 10^{19}$ cm^{-3} is fixed. The pressure $P_{\rm GB} = (\rho_t - \rho_{\rm liq})gL_0 = 0.6$ (mPa) is the sum of the gravity and buoyancy, where g is the gravitational acceleration, the thickness $L_0 = 100$ nm, and $\rho_t \approx 2.1$ g/cm^3 and $\rho_{\rm liq} \approx 1.50$ g/cm^3 are the densities of Teflon and bromobenzene, respectively. The results indicate that the curves of Casimir pressures for $N_a = 10^{18}$ and 10^{19} cm^{-3} are also overlapped, and the quantum trap is quite strong since the maximum of the restoring force is over 100 times of $P_{\rm GB}$. As N_a increases to 10^{21} cm^{-3}, the Casimir pressure tends to be more repulsive and the restoring force declines. Interestingly, a long-range repulsive can be obtained when $N_a = 2 \times 10^{21}$ cm^{-3}. Therefore, a switch from quantum trapping to its release is realized as the density N_a increases from 10^{19} to 2×10^{21} cm^{-3}. Another example of Casimir switching with $N_b = 10^{20}$ cm^{-3} is shown in Fig. 5(c). Again, there is a stable trapping when no bias is applied. However, the maximum of the restoring force increases as the active density N_a is depleted to 10^{18} and 10^{19} cm^{-3}, and the trapping stiffness can be slightly enhanced. As the density N_a increases to 10^{21} and 2×10^{21} cm^{-3}, however, the Casimir pressure becomes long-range repulsive. As a result, the switching from quantum trapping to its release can also be achieved by increasing the magnitude of N_a.

IV. THE FINITE TEMPERATURE EFFECT

The temperature of the system needs to be considered in a real configuration. Firstly, we assume the dielectric functions of the used materials are temperature independent. The integral over frequency ξ for 0 K approximation in Eq. (1) now should be written as a discrete summation [2]

$$\frac{\hbar}{2\pi}\int_0^\infty d\xi \leftrightarrow k_b T {\sum_{n=0}^{\infty}}', \tag{9}$$

where ξ is replaced by discrete Matsubara frequencies $\xi_n = 2\pi \frac{k_b T}{\hbar} n (n = 0, 1, 2, 3 \ldots)$, k_B is the Boltzmann's constant, T is the temperature of the system and the prime denotes a prefactor 1/2 for the term $n = 0$. The Casimir pressures

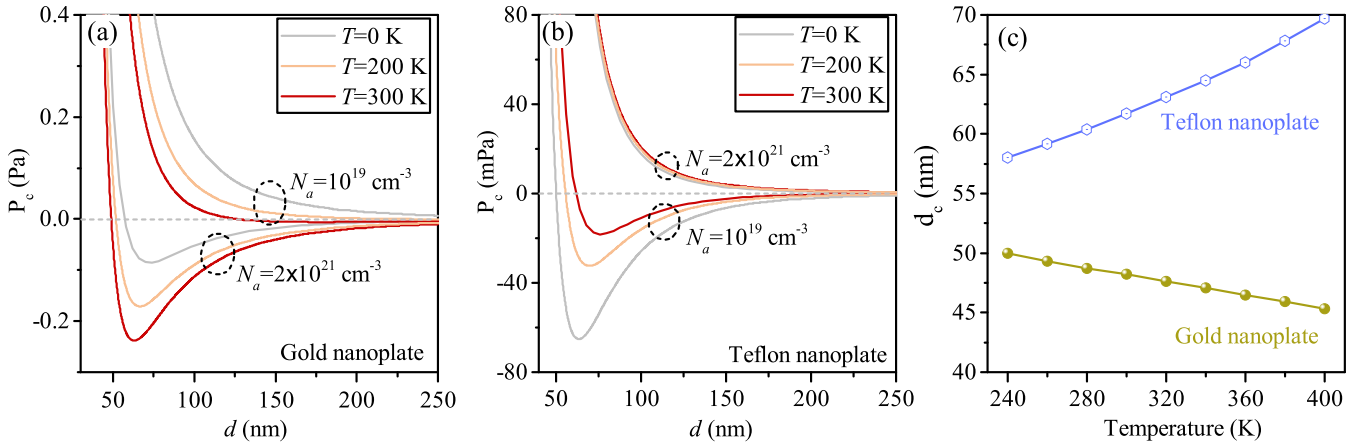

FIG. 6. The finite temperature effect for Casimir pressures. (a) A suspended gold nanoplate; (b) a suspended Teflon nanoplate. (c) The separation of quantum trapping as a function of temperature. In (a)–(c), the background density N_b is fixed at 10^{19} cm^{-3}, and the thicknesses parameters of the systems are kept the same as those in Figs. 4(b) and 5(b).

under different finite temperatures are shown in Figs. 6(a) and 6(b). For a gold nanoplate, the Casimir pressure tends to be more attractive as the temperature increases from 0 to 300 K. Comparing with the 0 K approximation, the maximum of the restoring force for the quantum trapping ($N_a = 2 \times 10^{21}$ cm^{-3}) increases considerably as the temperature is 300 K. Meanwhile, the trapping positions reduce slightly as the temperature increases. Interestingly, a Casimir equilibrium can be found for the release state ($N_a = 10^{19}$ cm^{-3}) with $T = 300$ K. However, this trapping state does not persist for a flipped-down case [39] because the restoring force is very weak (smaller than the P_{GB}). For a Teflon nanoplate, the maximum of the restoring forces for the trapping state ($N_a = 10^{19}$ cm^{-3}) reduces as the temperature increases from 0 to 300 K. Meanwhile, the trapping distances rises slightly as the temperature increases. Nonetheless, the Teflon nanoplate can be switched from quantum trapping to its release state for a finite temperature, and the calculation results do not change qualitatively comparing with the 0 K approximation. The temperature dependence of the Casimir equilibria for the state of quantum trapping is shown in Fig. 6(c). As the temperature T increases from 240 to 400 K, the critical distances d_c for a Teflon nanoplate grows from 58 to 70 nm (about 0.075 nm/K). Conversely, the distance d_c for a gold nanoplate drops from 50 to 45 nm (about -0.03 nm/K). Overall, the change of trapping distance is quite small for the temperature.

V. CONCLUSIONS

In summary, we study Casimir forces between gold/Teflon nanoplates and ITO-based MOS structures in a liquid environment. Our results suggest that the Casimir equilibria are determined, not only by the layer thicknesses in MOS structures but also by the carrier densities of ITO (gate-controllable). Under proper designs, a gold nanoplate can be stably trapped, and the trapping state can be released by decreasing the carrier density in the active layer of ITO. In addition to gold nanoplates, tunable Casimir equilibria for Teflon nanoplates are demonstrated. Instead, the quantum trapping can be tuned into a release state by increasing the carrier density in the active layer. Although we consider ITO films in this work, the concept of gate-tunable Casimir equilibria can be applied in other transparent conductive oxides such as aluminum-doped zinc oxide (AZO) and gallium-doped zinc oxide (GZO) [43]. The Teflon could also be replaced by other low-refractive-index materials (e.g., mesoporous silica [46]). Experimentally, the state-of-arts of the techniques for film deposition are mature, such as sputterings or vacuum thermal evaporation [47], pulsed laser depositions [48]. Our findings may have promising applications in MEMS/NEMS based on the quantum fluctuations of the electromagnetic field.

ACKNOWLEDGMENTS

This work is supported by the National Natural Science Foundation of China (Grants No. 11804288, No. 11704254, No. 61571386, and No. 61974127), and the Innovation Scientists and Technicians Troop Construction Projects of Henan Province. The research of L.G. is further supported by Nanhu Scholars Program for Young Scholars of XYNU.

[1] H. B. Casimir, Proc. Kon. Ned. Akad. Wet. **51**, 793 (1948).
[2] G. L. Klimchitskaya, U. Mohideen, and V. M. Mostepanenko, Rev. Mod. Phys. **81**, 1827 (2009).
[3] J. L. Garrett, D. A. T. Somers, and J. N. Munday, Phys. Rev. Lett. **120**, 040401 (2018).
[4] M. Liu, J. Xu, G. L. Klimchitskaya, V. M. Mostepanenko, and U. Mohideen, Phys. Rev. A **100**, 052511 (2019).
[5] S. E. Lyshevski, *MEMS and NEMS: Systems, Devices, and Structures* (CRC Press, Boca Raton, FL, 2018).
[6] E. Buks and M. L. Roukes, Phys. Rev. B **63**, 033402 (2001).

[7] H. Chan, V. Aksyuk, R. Kleiman, D. Bishop, and F. Capasso, Science **291**, 1941 (2001).

[8] L. M. Woods, D. A. R. Dalvit, A. Tkatchenko, P. Rodriguez-Lopez, A. W. Rodriguez, and R. Podgornik, Rev. Mod. Phys. **88**, 045003 (2016).

[9] F. S. S. Rosa, D. A. R. Dalvit, and P. W. Milonni, Phys. Rev. Lett. **100**, 183602 (2008).

[10] R. Zeng, Y. Yang, and S. Zhu, Phys. Rev. A **87**, 063823 (2013).

[11] J. S. Høye and I. Brevik, Phys. Rev. A **98**, 022503 (2018).

[12] R. Zhao, T. Koschny, E. N. Economou, and C. M. Soukoulis, Phys. Rev. B **83**, 075108 (2011).

[13] G. Song, R. Zeng, M. Al-Amri, J. Xu, C. Zhu, P. He, and Y. Yang, Opt. Express **26**, 34461 (2018).

[14] A. G. Grushin and A. Cortijo, Phys. Rev. Lett. **106**, 020403 (2011).

[15] W. Nie, R. Zeng, Y. Lan, and S. Zhu, Phys. Rev. B **88**, 085421 (2013).

[16] J. N. Munday, F. Capasso, and V. A. Parsegian, Nature (London) **457**, 170 (2009).

[17] P. J. van Zwol and G. Palasantzas, Phys. Rev. A **81**, 062502 (2010).

[18] S. J. Rahi and S. Zaheer, Phys. Rev. Lett. **104**, 070405 (2010).

[19] A. W. Rodriguez, J. N. Munday, J. D. Joannopoulos, F. Capasso, D. A. R. Dalvit, and S. G. Johnson, Phys. Rev. Lett. **101**, 190404 (2008).

[20] A. W. Rodriguez, A. P. McCauley, D. Woolf, F. Capasso, J. D. Joannopoulos, and S. G. Johnson, Phys. Rev. Lett. **104**, 160402 (2010).

[21] Y. Ye, Q. Hu, Q. Zhao, and Y. Meng, Phys. Rev. B **98**, 035410 (2018).

[22] R. Zhao, L. Li, S. Yang, W. Bao, Y. Xia, P. Ashby, Y. Wang, and X. Zhang, Science **364**, 984 (2019).

[23] E. M. Lifshitz, J. Exper. Theoret. Phys. USSR **29**, 94 (1956) [Sov. Phys.-JETP **2**, 73 (1956)].

[24] F. Chen, G. L. Klimchitskaya, V. M. Mostepanenko, and U. Mohideen, Phys. Rev. B **76**, 035338 (2007).

[25] C.-C. Chang, A. A. Banishev, G. L. Klimchitskaya, V. M. Mostepanenko, and U. Mohideen, Phys. Rev. Lett. **107**, 090403 (2011).

[26] A. A. Banishev, C.-C. Chang, R. Castillo-Garza, G. L. Klimchitskaya, V. M. Mostepanenko, and U. Mohideen, Phys. Rev. B **85**, 045436 (2012).

[27] G. L. Klimchitskaya and V. M. Mostepanenko, Phys. Rev. B **98**, 035307 (2018).

[28] C. Abbas, B. Guizal, and M. Antezza, Phys. Rev. Lett. **118**, 126101 (2017).

[29] M. Bordag, I. Fialkovskiy, and D. Vassilevich, Phys. Rev. B **93**, 075414 (2016).

[30] P. Rodriguez-Lopez, W. J. M. Kort-Kamp, D. A. R. Dalvit, and L. M. Woods, Nat. Commun. **8**, 1 (2017).

[31] W.-K. Tse and A. H. MacDonald, Phys. Rev. Lett. **109**, 236806 (2012).

[32] G. Torricelli, P. J. Van Zwol, O. Shpak, G. Palasantzas, V. B. Svetovoy, C. Binns, B. J. Kooi, P. Jost, and M. Wuttig, Adv. Funct. Mater. **22**, 3729 (2012).

[33] M. Sedighi, W. H. Broer, G. Palasantzas, and B. J. Kooi, Phys. Rev. B **88**, 165423 (2013).

[34] M. Boström, M. Dou, O. I. Malyi, P. Parashar, D. F. Parsons, I. Brevik, and C. Persson, Phys. Rev. B **97**, 125421 (2018).

[35] G. Torricelli, P. J. van Zwol, O. Shpak, C. Binns, G. Palasantzas, B. J. Kooi, V. B. Svetovoy, and M. Wuttig, Phys. Rev. A **82**, 010101(R) (2010).

[36] E. G. Galkina, B. A. Ivanov, S. Savel'ev, V. A. Yampol'skii, and F. Nori, Phys. Rev. B **80**, 125119 (2009).

[37] I. Pirozhenko and A. Lambrecht, Phys. Rev. A **77**, 013811 (2008).

[38] R. Castillo-Garza, C.-C. Chang, D. Jimenez, G. L. Klimchitskaya, V. M. Mostepanenko, and U. Mohideen, Phys. Rev. A **75**, 062114 (2007).

[39] L. Ge, X. Shi, Z. Xu, and K. Gong, Phys. Rev. B **101**, 104107 (2020).

[40] A. V. Krasavin and A. V. Zayats, Phys. Rev. Lett. **109**, 053901 (2012).

[41] Y.-W. Huang, H. W. H. Lee, R. Sokhoyan, R. A. Pala, K. Thyagarajan, S. Han, D. P. Tsai, and H. A. Atwater, Nano Lett. **16**, 5319 (2016).

[42] G. T. Papadakis, B. Zhao, S. Buddhiraju, and S. Fan, ACS Photonics **6**, 709 (2019).

[43] V. E. Babicheva, A. Boltasseva, and A. V. Lavrinenko, Nanophotonics **4**, 165 (2015).

[44] T. Zhan, X. Shi, Y. Dai, X. Liu, and J. Zi, J. Phys.: Condens. Matter **25**, 215301 (2013).

[45] H. S. Sehmi, W. Langbein, and E. A. Muljarov, Phys. Rev. B **95**, 115444 (2017).

[46] M. Dou, F. Lou, M. Boström, I. Brevik, and C. Persson, Phys. Rev. B **89**, 201407(R) (2014).

[47] Z. Wu, L. Wang, H. Wang, Y. Gao, and Y. Qiu, Phys. Rev. B **74**, 165307 (2006).

[48] G. V. Naik, V. M. Shalaev, and A. Boltasseva, Adv. Mater. **25**, 3264 (2013).